Vertically Aligned and Continuous Nanoscale Ceramic–Polymer Interfaces in Composite Solid Polymer Electrolytes for Enhanced Ionic Conductivity

Xiaokun Zhang,[†,‡,⊥] Jin Xie,[†,⊥] Feifei Shi,[†] Dingchang Lin,[†] Yayuan Liu,[†] Wei Liu,[†] Allen Pei,[†] Yongji Gong,[†] Hongxia Wang,[†] Kai Liu,[†] Yong Xiang,*[,‡] and Yi Cui*[,†,§]

[†]Department of Materials Science and Engineering, Stanford University, Stanford, California 94305, United States

[‡]School of Materials and Energy, University of Electronic Science and Technology of China, Chengdu, Sichuan 611731, People's Republic of China

[§]Stanford Institute for Materials and Energy Sciences, SLAC National Accelerator Laboratory, 2575 Sand Hill Road, Menlo Park, California 94025, United States

S *Supporting Information*
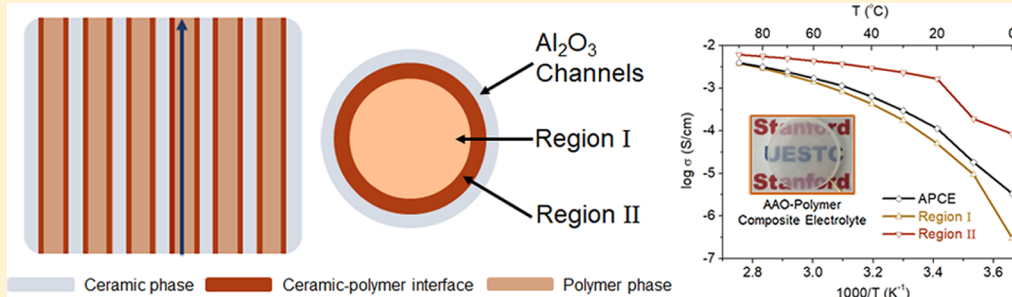
ABSTRACT: Among all solid electrolytes, composite solid polymer electrolytes, comprised of polymer matrix and ceramic fillers, garner great interest due to the enhancement of ionic conductivity and mechanical properties derived from ceramic–polymer interactions. Here, we report a composite electrolyte with densely packed, vertically aligned, and continuous nanoscale ceramic–polymer interfaces, using surface-modified anodized aluminum oxide as the ceramic scaffold and poly(ethylene oxide) as the polymer matrix. The fast Li^+ transport along the ceramic–polymer interfaces was proven experimentally for the first time, and an interfacial ionic conductivity higher than 10^{-3} S/cm at 0 °C was predicted. The presented composite solid electrolyte achieved an ionic conductivity as high as 5.82×10^{-4} S/cm at the electrode level. The vertically aligned interfacial structure in the composite electrolytes enables the viable application of the composite solid electrolyte with superior ionic conductivity and high hardness, allowing Li–Li cells to be cycled at a small polarization without Li dendrite penetration.

KEYWORDS: *Lithium batteries, composite solid polymer electrolytes, ionic conductivity, ceramic–polymer interfaces, vertically aligned nanostructures*

Lithium-ion batteries have been the dominant energy storage technology for portable electronics, electric vehicles, and drones, thanks to their high energy and power densities, low self-discharge rates, and long cycle life.[1−3] However, safety issues derived from flammable liquid electrolytes and lithium dendrite growth remain as challenges for lithium batteries.[4−6] Solid electrolytes have attracted significant attention from academic and industrial communities due to their inherent nonflammability and mechanical hardness and are a promising approach to enable high capacity lithium metal anodes.[7−15] While solid ceramic electrolytes is an exciting direction to pursue,[12,13,16−19] solid polymer electrolytes (SPE) offer another promising approach because of their excellent manufacturability and lightweight.[5−8,20]

One of the key challenges for SPE is to enhance their ionic conductivity within the operation temperature range of lithium

batteries.[21] To date, introducing nanoscale inorganic fillers into the polymer matrix of SPE to form a composite solid polymer electrolyte (CSPE) is one of the most effective strategies to enhance the ionic conductivity.[22−27] A few studies on CSPE have demonstrated that the enhancement of ionic conductivity in CSPE originates from the interactions at the interface between ceramic fillers and polymer matrix.[27−36] First, polymer chains are anchored onto surface sites of inorganic fillers through physical and/or chemical interactions, resulting in an amorphous-rich area around the ceramics fillers which can transport Li^+ in a fast manner.[27−30] Second, the strong Lewis acid−base interaction between the surface chemical groups of
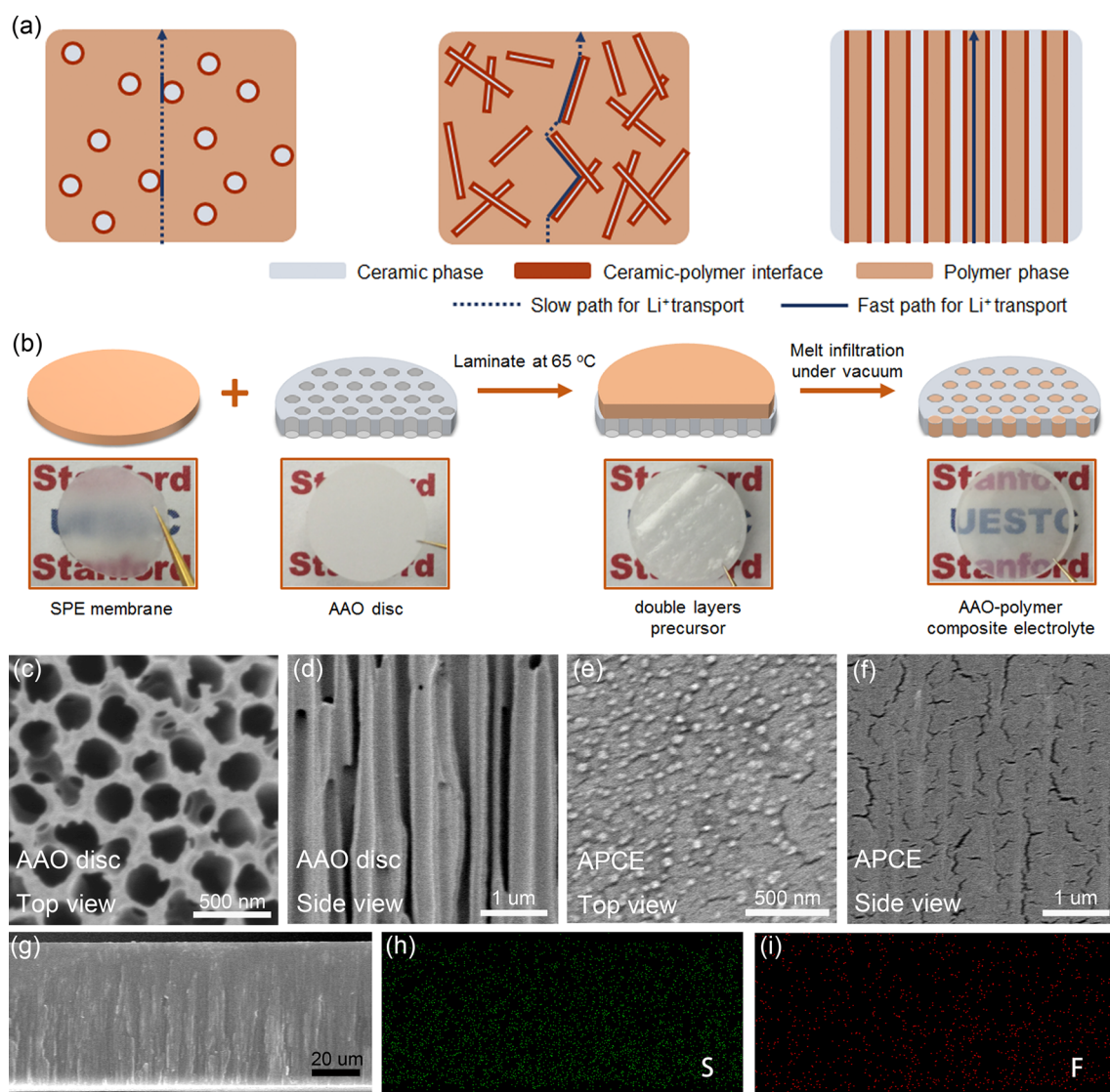
Figure 1. Conceptual design, fabrication procedures, and materials characterization of AAO-polymer composite electrolyte. (a) Schematics of composite solid polymer electrolyte with three types of geometrical structures of ceramic−polymer interface; (b) schematics of fabrication procedures of AAO-polymer composite electrolyte; (c−f) SEM characterizations of pristine AAO (top view and side view) and SPE infiltrated AAO (top view and side view); (g−i) EDX mapping of S and F elements across the entire thickness of AAO-polymer composite electrolyte.

inorganic fillers and ion species in the polymer matrix facilitates the lithium salt dissociation. The concentration of free Li$^+$ at the interface can be increased when anions in the lithium salt are attracted to the surface of inorganic fillers.[14,31−34] Third, the interaction between ceramic and polymer leads to possible Li$^+$-conductive substructures of the polymer matrix via influence on the local conformation of polymer segments.[35−37] To summarize, fast paths for Li$^+$ transport can be achieved by designing an ideal interface between ceramic fillers and polymer matrix.

Considering these beneficial interfacial effects, we propose that using inorganic fillers with different morphologies leads to different inorganic−polymer interfacial geometries, which could result in significant differences in ionic conductivity enhancement in CSPE (Figure 1a). For nanoscale fillers with low aspect ratios, such as nanoparticles (NPs),[27,29,30] the fast transport paths are short-ranged and isolated; thus the ionic conductivity enhancement is limited. On the other hand, nanoscale fillers with high aspect ratios, such as nanowires (NWs), show stronger ionic conductivity enhancement than NPs.[25,38] This is

because NWs provide considerably prolonged fast transport pathways for Li$^+$. However, the fast transport pathways along nanowire/polymer interfaces in NWs-based CSPE are randomly oriented and discontinuous. Additionally, the Li$^+$ conduction at filler−filler interfaces, such as NW−NW crossing junctions, is poor.[26,39] Very recently, a SPE with embedded horizontally aligned ceramic nanowires without crossing junctions has been developed to measure the interfacial ionic conductivity, giving an astonishing number of 10^{-2} S/cm at the interface, similar to the liquid ionic conductivity.[39] However, the absolute value of ionic conductivity for the CSPE with aligned ceramic nanowires is limited by the low content of fillers in the polymer (∼3 wt %), which only provides a limited NW−polymer interfacial area for fast transport of Li$^+$. Moreover, real batteries would require vertical (instead of horizontal) alignment and high loading of nanowires in the polymer electrolyte to realize continuous and abundant interfacial ion-conducting pathways directly bridging the cathode and anode.

In this work, we demonstrate an anodized aluminum oxide (AAO)−polymer composite electrolyte (APCE) with vertically aligned and continuous ceramic−polymer interfaces (as depicted in right of Figure 1a) by filling solid polymer electrolyte into the nanochannels of AAO. As a demonstration, poly(ethylene oxide) (PEO)-LiTFSI SPE was chosen as a model system. Al_2O_3, an inert filler which cannot conduct Li^+ by itself, was used to make sure the ionic conductivity enhancement observed in this study comes solely from the interfacial interaction between the polymer matrix and ceramic fillers. SPE based on PEO (M_w 300 000) and LiTFSI was introduced into the nanochannels of AAO discs by a melt infiltration method,[40,41] as illustrated in Figure 1b. Vertical, continuous, and non-tortuous ceramic−polymer interfaces were formed along alumina nanochannels. AAO discs have nanoscale pore sizes and a porosity higher than 50%, ensuring plentiful ceramic surfaces exposed to polymer electrolytes. Because of the interfacial effects mentioned above, the ionic conductivity at room temperature (RT) of APCE was 1−2 orders of magnitude higher than filler-free SPE and about 5 times higher than its CSPE counterparts based on NP- or NW-fillers. Note that the ionic conductivity of APCE is determined based on the polymer part area, because the framework of Al_2O_3 does not contribute to the Li^+ conductance. Furthermore, the surface chemistry of AAO can be easily changed by surface chemical modification using atomic layer deposition (ALD), which provides us the flexibility of modifying the ceramic−polymer interactions at the interface. Through appropriate interfacial modification and polymer molecular weight optimization, the ionic conductivity at RT achieved in this study was as high as 5.82×10^{-4} S/cm. To the best of our knowledge, this is the highest ionic conductivity achieved in polymer-based solid electrolytes (Table S1). The interfacial effects on ionic conductivity enhancement in APCE is further supported by deducing the ionic conductivity of the interfacial region and studying the quantitative relationship between diameters of AAO nanochannels and measured ionic conductivities. Moreover, with the mechanically stable and heat resistant AAO core, the overall mechanical, thermal, and long-term stability of APCE is improved compared to SPE.

Results and Discussion. *Materials Fabrication and Characterization.* The fabricating procedures of APCE are schematically illustrated in Figure 1b. A PEO-LiTFSI SPE membrane, which was prepared by a doctor blading process using an acetonitrile solution containing PEO and LiTFSI, was thermally laminated onto the top of an AAO disc. The SPE membrane was then melted and infiltrated into nanochannels of AAO at 215 °C under vacuum. The melt infiltration took 12 h for ensuring the nanochannels were completely filled and the vertically aligned continuous ceramic−polymer interfaces were well-formed.

Vertically aligned nanochannels in the pristine AAO disc have an average diameter of 200 nm (Figure 1c,d). Nanochannels were fully filled by polymer electrolyte after melt infiltration (Figure 1e,f). The remaining polymer on the surface of the AAO disc was removed after melt infiltration (Figure 1e,g). The intimate contact of polymer electrolyte and Al_2O_3 nanochannels seen in Figure 1f confirms the formation of desired continuous ceramic−polymer interfaces. The EDX mapping of elements (S and F) derived from LiTFSI across the 60 μm thick APCE further confirms the uniform distribution of polymer electrolyte throughout the nanochannels (Figure 1h,i). The effectiveness of the melt infiltration process used here is

also evidenced by the fact that the APCE sample became optically translucent while the pristine AAO disc was white (Figure 1b). This color change was attributed to the reduction of light scattering by hollow nanochannels when they were fully filled.

In the case of APCE with modified ceramic−polymer interface, a layer of AlF_3 was coated onto the wall of nanochannels by ALD before melt infiltration of SPE. TiF_4 and $AlCl_3$, the source of F and Al, respectively, were alternately introduced to AAO substrates heated at 250 °C. One hundred ALD cycles were applied to obtain a uniform and sufficient coating of 10 nm thick AlF_3.[42] The top view SEM image and EDX elemental mapping of F at the cross section of the AAO disc after AlF_3 deposition (Figure S1) indicates that the surface modification did not change the diameter of nanochannels significantly and the coating of AlF_3 on the wall of nanochannels is uniform.

Ionic Conductivity Enhancement by Structural Design of Ceramic−Polymer Interface. To study the influence of the geometrical structure of the ceramic−polymer interface on the ionic conductivity of composite electrolyte, electrochemical impedance spectroscopy (EIS) measurements of four types of solid electrolytes including pure SPE, CSPE with random dispersed nanoparticles (CSPE-NPs), CSPE with random dispersed nanowires (CSPE-NWs), and APCE with vertically aligned and continuous nanoscale ceramic−polymer interface were conducted at different temperatures with two gold blocking electrodes (Figure 2a,b). Each EIS profile comprises
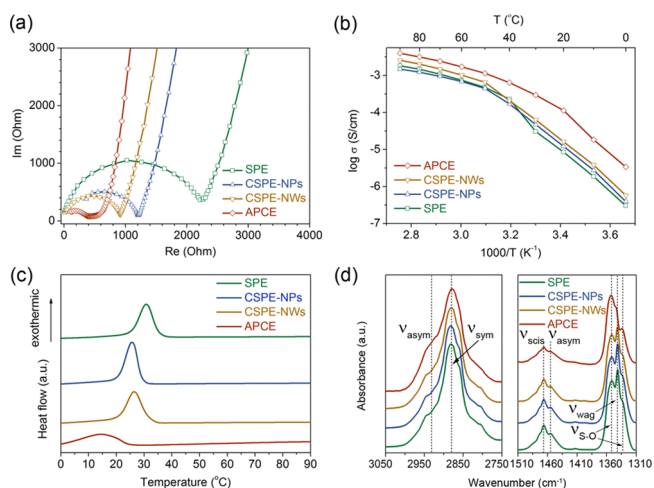

Figure 2. Characterizations of SPE, CSPE-NPs, CSPE-NWs, and APCE. (a) Electrochemical impedance spectra measured at room temperature, (b) temperature dependence of ionic conductivities, (c) DSC traces recorded during cool down, and (d) FTIR absorption spectra taken at room temperature inside of a glovebox.

a semicircle and a spike, which represent the impedance characteristics derived from the electrolyte bulk and the electrolyte−electrode interface, respectively.[25,38] The ionic conductivities of solid electrolytes were calculated based on the thickness of solid electrolyte, effective electrolyte−electrode contact area, and the bulk resistance represented by the intercept of the extended semicircle on the real axis. At RT, APCE based on PEO (M_w 300 000) and LiTFSI had an ionic conductivity of 1.79×10^{-4} S/cm, which was 1 order of magnitude higher than the corresponding SPE (1.69×10^{-5} S/cm), and about 4 times higher than corresponding CSPE-NPs

(3.13 × 10^{-5} S/cm) and CSPE-NWs (4.13 × 10^{-5} S/cm). Furthermore, APCE showed a remarkable ionic conductivity enhancement over the temperature range from 0 to 90 °C. The bend curves in Figure 2b indicate that all the solid electrolytes involved in this study possess a Vogel−Tammann−Fulcher (VTF) behavior of temperature dependence of ionic conductivities.[43] It confirms that conducting ions reside in the polymer phase and they pass through the polymer matrix but not the ceramic phase for both CSPE and APCE. We propose that both CSPE and APCE have two Li$^+$ conducting pathways. The first one is regular Li$^+$ transport by ether oxygen-assisted hopping or polymer segmental motion. The second pathway is enhanced Li$^+$ transport along the ceramic−polymer interfaces. SPE has the lowest conductivity because it is inherently semicrystalline and the Li$^+$ conduction can only take place through oxygen-assisted hopping or polymer segmental motion. The enhanced ionic conductivities in CSPE are because the ceramic fillers decreased the degree of polymer crystallinity, increased free Li$^+$ concentration, and provided fast pathways for Li$^+$ transport around ceramic−polymer interfaces. The specific interface area, which is the interfacial area per unit volume of composite electrolyte, is another parameter which may affect the ionic conductivity for CSPE beyond the geometrical structure of the ceramic−polymer interface. The specific interface area of composite electrolytes involved in this study are calculated and summarized (Note S1). CSPE-NWs showed higher conductivities than CSPE-NPs, which can be attributed to the fact that NWs provide a long-range continuous interface with high aspect ratio. Among the four electrolytes, APCE had the highest ionic conductivity. Notably, while the specific interface area of APCE (1.1 × 10^5 cm^{-1}) is only one-third of the specific interface area of CSPE-NWs (3.0 × 10^5 cm^{-1}), the ionic conductivity of the former is 4.3 times higher than the later. Moreover, the activation energies of SPE, CSPE-NPs, CSPE-NWs, and APCE were calculated through VTF fitting of the temperature dependence of ionic conductivities shown in Figure 2b (see details in Note S2). SPE has an activation energy of 0.042 eV, which is in consistent with the report in literature.[44] The activation energy of APCE is significantly reduced to 0.027 eV, which is due to the fast Li$^+$ transport along the vertically aligned continuous interfaces.[39,45−47] The activation energies of CSPE-NPs (0.059 eV) and CSPE-NWs (0.040 eV) are close to SPE. This can be attributed to the fact that their fast paths for Li$^+$ transport are discontinuous and their impact on the overall ionic conductivity of composite electrolytes is limited in terms of activation energy. The superior ionic conductivity and lower activation energy in APCE demonstrate the importance of vertically aligned continuous ceramic−polymer interfaces for maximizing the interfacial effects on enhancing ionic conductivity in ceramic−polymer composite electrolytes.

It is worth to note that APCE possesses significantly higher ionic conductivities than SPE and conventional CSPE from 0 to 30 °C, which coincides with the operating temperature range for lithium batteries typically used in portable electronics, electrical vehicles, and drones. This is of great importance for developing practical lithium batteries. Figure 2c shows differential scanning calorimetry (DSC) traces of SPE, CSPE-NPs, CSPE-NWs, and ACPE recorded during cooling down from 90 to 0 °C. The crystallization temperature of SPE was 30 °C which is consistent with the report in literature.[48] CSPE-NPs and CSPE-NWs possessed a lower crystallization temperature at around 25 °C. For comparison, the crystallization

temperature of APCE dramatically decreases to 15 °C, which is consistent with the precipitous drop of APCE's measured ionic conductivity due to the phase transition from amorphous to semicrystalline state below 20 °C. In addition, APCE exhibited a much lower crystallinity of 14.7% than the polymer in SPE (22.7%) and CSPE (20.0% and 19.7% for the NPs- and NWs-based, respectively) at temperatures lower than its crystallization temperature. The details of the calculation of the degree of crystallinity can be seen in Note S3. The significantly decreased crystallinity and crystallization temperature should contribute to APCE's superior ionic conductivities from 0 to 30 °C.

The superior ionic conductivity enhancement of APCE is still substantial but less pronounced when T > 30 °C. This is because (i) the Lewis acid−base interaction at the ceramic−polymer interface facilitates lithium salt dissociation,[34] but the intrinsic high dissociation degree of lithium salts at higher temperature make the interfacial effect less pronounced, (ii) the polymer matrix is in an amorphous state no matter if there are ceramic fillers or not, as indicated by DSC (Figure 2c) when T > 30 °C, and (iii) the mobility of polymer chains is so high that the Li$^+$-conduction-promoting substructures of polymer chains may fade away. Thus, the structure- and substructure-induced ionic conductivity enhancement was eclipsed by the temperature effect. It should be noted that CSPE-NPs had lower ionic conductivities than ceramic-free SPE when temperature exceeded 60 °C because the inert nanoparticles may aggregate and form large barriers for Li$^+$ transport when the viscosity of the polymer matrix decreases. This indicates that APCE with a structure-stable ceramic phase may exhibit more stable performance than conventional CSPE with randomly dispersed ceramic fillers at high temperatures.

To study the interfacial effect on the segmental structure in composite electrolytes, Fourier transform infrared spectroscopy (FTIR) spectra of SPE, CSPE-NPs, CSPE-NWs, and ACPE were measured at RT (Figure 2d). The typical bands of PEO at 2930, 2885, 1465, 1450, and 1341 cm^{-1} are attributed to asymmetric stretching, symmetric stretching, scissoring, asymmetric bending, and wagging vibrations of C−H, respectively.[49−52] The bands at 1354 and 1333 cm-1 are assigned to S−O from TFSI$^-$.[53] The C−H stretching band is quite sensitive to the extent of lithium salt complexation. The asymmetrical C−H stretching in the APCE had larger absorption than that in the SPE, CSPE-NPs, and CSPE-NWs, which indicates the disorder degree of the polymer matrix in APCE is much higher.[54,55] We also checked the C−O ether functional group region in the FTIR spectra (Figure S2). The peaks of ether functional group in SPE locate at 1094 and 1052 cm^{-1} in SPE. With the addition of nanoparticle or nanowires, this pair of peaks shift to 1096 and 1054 cm^{-1}. In the APCE, the 200 nm pore cause an even more obvious shift to 1112 and 1058 cm^{-1}. The well-aligned and continuous ceramic−polymer interfaces in APCE may amplify the polymer segment anchoring and cross-linking effects of ceramic−polymer interactions (also see Figure S3 for the lithium salt free case), which may in turn influence polymer chain conformation and lead to formation of Li$^+$-conductive substructures at the interface, thus resulting in superior ionic conductivities.

Ionic Conductivity Enhancement by Interfacial Chemical Modification. In addition to the effects from optimized geometrical structures, the Lewis acid characteristics and dielectric properties of the ceramic phase also play critical roles in ionic conductivity enhancement and follow the general

criteria from conventional ceramic−polymer composite electrolytes. For example, strong Lewis acid−base interaction leads to an enhanced level of lithium salt dissociation and thus a higher ionic conductivity. Therefore, the ceramic−polymer interfacial interactions in APCE can be boosted by modifying the continuous surface of Al_2O_3 nanochannels in AAO with an ultrathin layer of a strong Lewis acid, such as AlF_3.[56−58] As depicted in Figure 3a, surface modification of nanochannels in
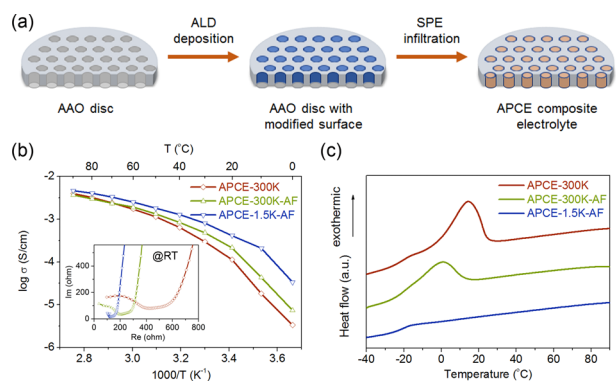

Figure 3. The strategy to improve the ionic conductivity of APCE. (a) Schematic illustrations of surface modification of a AAO disc for APCE; (b) Arrhenius plots of ionic conductivity and electrochemical impedance spectra measured at room temperature; and (c) DSC traces recorded during cool down of APCE: red, bare AAO with PEO (M_w 300 000); green, AlF_3-coated AAO with PEO (M_w 300 000); blue, AlF_3-coated AAO with PEG (M_w 1500).

AAO discs was carried out by ALD of AlF_3. The ionic conductivity at room temperature of APEC with AlF_3 coated AAO discs and PEO (M_w 300 000) (APCE-300K-AF) was 3.50 × 10^{-4} S/cm, which is doubled that of its counterpart without AlF_3 coating (1.79 × 10^{-4} S/cm for APCE-300K) (Figure 3b). It should be noted that the incomplete semicircle in Figure 3b is because the instrumental limitation at high frequency for the APCE samples tested here. DSC traces shown in Figure 3c demonstrate that APCE-300K-AF possesses a lower crystallization temperature and crystallinity (9.79%) than APCE-300K without surface modification (14.7%). However, there is no obvious difference of absorbance intensity observed in the FTIR spectra of APCE with and without AlF_3 surface modification (Figure S4), indicating that surface modification does not significantly influence the anchoring or cross-linking process between the ceramic surface and polymer segments. The improvement of ionic conductivity arising from surface modification is attributed to the fact that AlF_3, as a strong Lewis acid, leads to intense Lewis acid−base interaction at the ceramic−polymer interfaces and results in higher Li^+ concentration around the interface.[31−34] This hypothesis was also supported by the slightly increased ionic transport numbers of APCE based on AlF_3 modified AAO as compared to that based on pristine AAO (Note S4). The lower crystallization temperature and crystallinity of APCE-300K-AF should be attributed to the fact that AlF_3-facilitated LiTFSI dissociation not only provides more free Li^+ as conducting carriers but also provides more $TFSI^-$ to form anion-polymer complexes, which act as plasticizers in the polymer matrix. The decreased slope of the Arrhenius plots of APCE based on AlF_3-coated AAO compared to that of APCE based on pristine AAO indicates that the activation energy of APCE was reduced by AlF_3 surface modification (Figure 3b and Figure S5b). This

suggests that surface modification by the strong Lewis acid AlF_3 effectively decreased the energy of lithium salt dissociation in APCE.

As mentioned above, polymer segmental motion-assisted Li^+ transport is also one of the most important conducting mechanisms in APCE. Generally, poly(ethylene glycol) (PEG) with lower molecular weight has lower crystallization temperature. However, polymers with low molecular weight may lead to poor mechanical strength in conventional composite electrolytes. For APCE, benefiting from the excellent stiffness of the AAO as a host for polymers, PEG can be applied to significantly improve ionic conductivity without sacrificing mechanical strength as a whole. APCE-1.5K-AF was prepared by infiltrating polymer electrolyte based on PEG (M_w 1500) and LiTFSI into AlF_3-modified AAO. APCE-1.5K-AF exhibits much higher ionic conductivities than APCE based on high molecular weight PEO (Figure 3b), benefiting from the drastically reduced crystallinity of polymer matrix (Figure 3c). The ionic conductivity at RT of APCE-1.5K-AF was as high as 5.82 × 10^{-4} S/cm. It is worth noting that this high ionic conductivity at RT achieved in APCE-1.5K-AF, to the best of our knowledge, is the highest value reported for polymer−ceramic composite solid electrolytes (Table S1).

The Effects of Vertically Aligned and Continuous Nanoscale Interfaces on Ionic Conductivity Enhancement. In APCE, only the polymer phase contributes to Li^+ conduction as Al_2O_3 itself is not a Li^+ conductor. As previously reported, the Li^+ conductivity of the polymer matrix near the ceramic−polymer interface may be significantly enhanced.[39] We therefore divided the nanochannel-embedded polymer cylinder into two regions: region I, which is the bulk part far from the ceramic−polymer interface, and region II, which is the interfacial layer formed at the surface of the ceramic phase, as depicted in Figure 4a. The overall ionic conductance of APCE depends on the ionic conductivities of region I, region II, and the thickness of interfacial layer. On the basis of the assumption that the ionic conducting and polymer segmental behaviors in these two regions abide by the VTF model, their ionic conductivities and the thickness of the interfacial layer can be calculated separately through a nonlinear data fitting of the measured ionic conductivity of APCE at different temperatures (for details see Note S5). Region II possesses higher ionic conductivities than region I over the temperature range from 0 to 90 °C and much lower activation energy as indicated by the significantly decreased slope of the Arrhenius plots (Figure 4b). These results suggest that fast paths for Li^+ transport with particular conducting mechanisms form along the vertically aligned and continuous ceramic−polymer interfaces. The interfacial ionic conductivity can be further improved by chemical modification of the ceramic surface and by using polymer with lower molecular weight (Figure 4c). APCE-1.5K-AF was calculated to have a high interfacial ionic conductivity of 6.47 × 10^{-3} S/cm at 30 °C, and the value is consistently higher than 10^{-3} S/cm even at 0 °C. The temperature dependence of the calculated interfacial ionic conductivity is consistent with DSC measurement results. For example, the sharp drop of APCE-300 K's interfacial ionic conductivity between 20 and 10 °C may be attributed to solidification of the polymer matrix, which is consistent with its thermal transition at 15 °C observed in the DSC trace (Figure 2c). Interestingly, region I showed higher ionic conductivities than pure SPE, although its Li^+ conducting behavior is intuitively considered to be similar to that in ceramic-free bulk SPE because it is far from
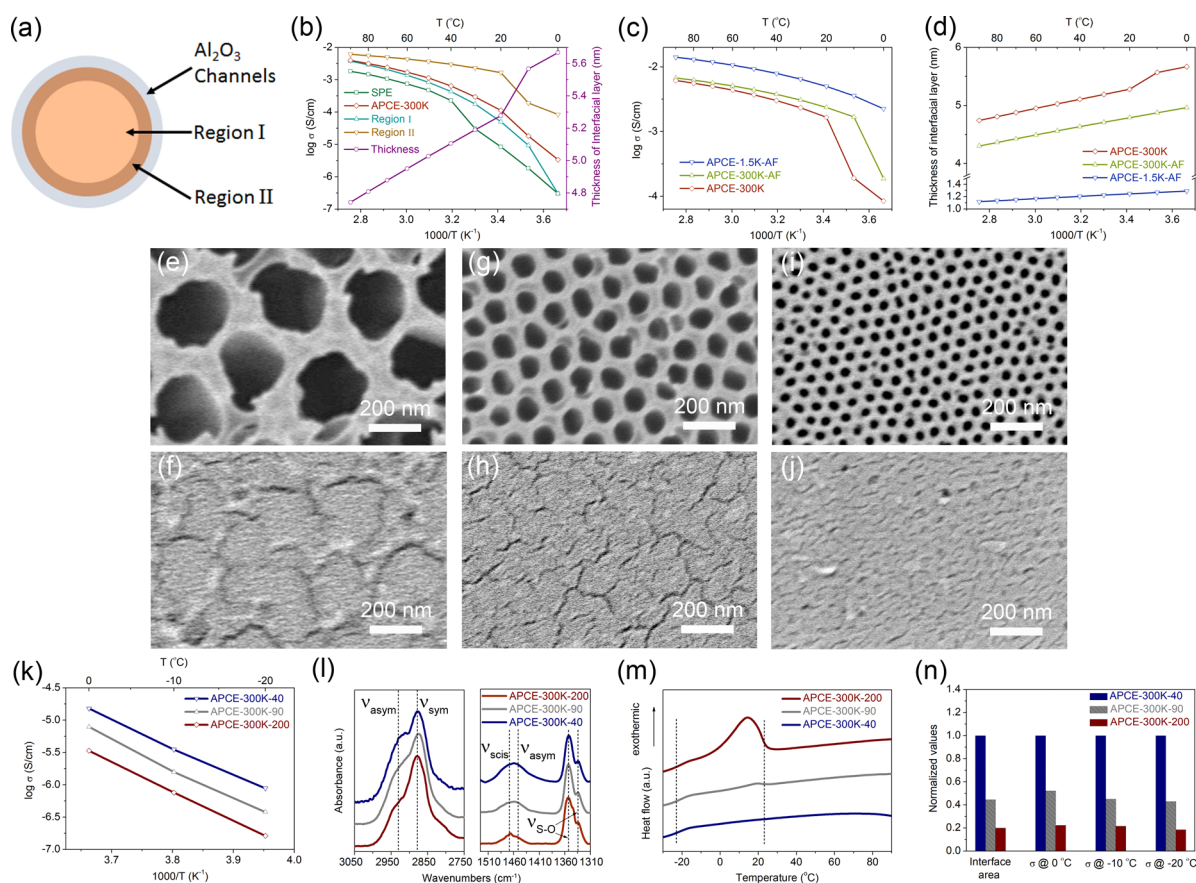
Figure 4. Analysis of interfacial ionic conductivity in APCE. (a) Schematics of polymer electrolyte in individual nanochannel of the AAO disc; (b) calculated ionic conductivities of region I and region II in APCE-300 K, and the thickness of interfacial layer between polymer and ceramic phase (region II), together with measured ionic conductivities of APCE-300 K and conventional bulk SPE for comparison; (c) interfacial ionic conductivities and (d) the thickness of interfacial layer of APCE based on AAO discs with or without surface modification and polymers with different molecular weight; (e−j) SEM images of AAO discs with pore size of 200 nm (e,f), 90 nm (g,h), and 40 nm (i,j) before (upper) and after (below) SPE infiltration; (k) Arrhenius plots of ionic conductivity, (l) FTIR absorption spectra, (m) DSC traces, and (n) normalized interface area and ionic conductivities at 0 °C, −10 °C, and −20 °C of AAO−polymer composite electrolyte based on AAO discs with different pore sizes, respectively.

the ceramic−polymer interface. Therefore, the effects of the ceramic−polymer interface on ionic conductivity enhancement in APCE can be summarized as follows: First, the vertically aligned and continuous structure of the interface makes the contribution of fast Li$^+$ transport paths along ceramic−polymer interfaces to the overall ionic conductance more pronounced. Second, nanochannels surrounded by the continuous interfaces may effectively restrict the crystallization of polymer matrix due to spatial confinement[59,60] and thus lead to a much higher ionic conductivity for the bulk part in APCE than that of conventional bulk SPE.

Besides interfacial ionic conductivity, the thickness of interfacial layer is another factor which influences the contribution of the interface to the overall ionic conductance of APCE. The thickness of the interfacial layer increases as temperature decreases (Figure 4b,d) because the mobility of polymer segments is reduced and more polymer chains are attached to the ceramic surface. Additionally, the interfacial layer thickness is also influenced by the interface modification and polymer molecular weight (Figure 4d). A strong Lewis acid on the ceramic surface, such as AlF$_3$, leads to a slightly thinner interfacial layer. This is because the strong Lewis acid facilitates LiTFSI dissociation and provides more TFSI- to form anion−polymer complexes, which may compete with the anchoring

and cross-linking process between the ceramic surface and polymer segments. When PEO (M_w 300 000) is replaced by PEG (M_w 1500) in APCE, a more notable decrease in the interfacial layer thickness can be deduced through data fitting and calculation. This is because the limited number of chemical sites on the ceramic surface only allows a limited number of polymer segments to attach, and the radius of gyration of PEG (<3 nm)[61,62] is much shorter than that of PEO (> 30 nm).[63,64]

Considering the temperature dependence of the calculated ionic conductivities of region I and region II, and the thickness of the interfacial layer (Figure 4d), Li$^+$ transport along the interfaces should contribute to the overall Li$^+$ conductance in APCE more and more as temperature decreases. For example, region II (8.44×10^{-5} S/cm, 9.66×10^{-3} cm^2) has 280.40 times the ionic conductivity and 0.12 times the cross-sectional area of Region I (3.01×10^{-7} S/cm, 7.80×10^{-2} cm^2) at 0 °C. In other words, the ionic conductance of region II is about 34 times of region I. At lower temperatures, Li$^+$ conduction along the vertically aligned and continuous interfaces should dominate Li$^+$ conduction in APCE because region I possesses a much steeper slope of the Arrhenius plot than region II. This is also supported by the calculation of activation energies of the composite electrolytes before and after melting (Note S2). For APCE, the activation energies before melting is one-half of that

after melting. Meanwhile, SPE, CSPE-NPs, and CSPE-NWs present a higher activation energy before melting, which is typical for polymer electrolytes.[44] The extraordinary temperature dependence of APCE's activation energy implies that the Li$^+$ conduction in APCE at a low temperature, such as at 0 °C, is dominated by a conduction mechanism different than that of SPE or conventional CSPE, which in this case is induced by the vertically aligned and continuous interfaces. Thus, AAO discs with reduced pore size, which can provide larger ceramic−polymer interface area per electrolyte volume (Table S2) for forming the fast paths of Li$^+$ transport, should further improve ionic conductivity of APCE at 0 °C and lower temperatures. We measured the ionic conductivities of APCE with nano-channels of diameters 200, 90, and 40 nm (denoted as APCE-300K-200, APCE-300K-90, and APCE-300K-40 below), respectively. The interfacial area per volume of polymer for APCE with different nanochannel diameters is calculated (see details in Note S6). The morphology characterizations of APCE demonstrate that the nanochannels were fully filled with polymers for AAO with different pore sizes (Figure 4e−j and Figure S6). In the low temperature range from 0 to −20 °C, the ionic conductivities of APCEs increased with increased interface area (Figure 4k). FTIR spectra showed that the intensity of asymmetrical vibrations of C−H increased as the diameters of nanochannels decreased (Figure 4l). However, there is no obvious peak shift for C−O vibration, except a little bit shape variation (Figure S2b). DSC traces shown in Figure 4m demonstrated that the degree of crystallinity of polymer matrix in APCE decreases as the nanochannel diameter decreases. According to Note S3, the crystallinity of the APCE with the pore size of 200, 90, and 40 nm is 14.7%, 3.36%, and 1.96%, respectively. The endothermic peak is not conspicuous for the DSC trace of APCE-330K-40 (blue line) due to the lowest crystallinity and content of polymer. The latter is because both porosity and pore size of AAO discs in APCE-300K−40 is smallest (See Note S1 and Table S2). However, we still can observe a bulge around −20 °C from the DSC trace of APCE-300K-40. Meanwhile, the variation of polymer chain organization and crystallinity with changing nanochannel diameter demonstrates that the smaller diameter of nanochannels leads to a larger volume ratio of region II, which in turn induces more obvious interfacial effects. Figure 4n compares the normalized interfacial area and ionic conductivities of APCE-300K-200, APCE-300K-90, and APCE-300K-40. One can see that the ratio of normalized ionic conductivities at three temperatures were all proportional to their normalized interface area. This quantitative result experimentally confirms that the fast paths for Li$^+$ transport are formed along the vertically aligned continuous interface in APCE.

The Feasibility and Stability of AAO−Polymer Composite Electrolyte. The APCE and SPE were tested in coin cells with a symmetrical Li/electrolyte/Li design. With a current density of 0.25 mA/cm^2, the cell based on APCE-300 K showed significantly lower overpotential (∼30 mV) than that of the cell based on SPE (∼70 mV) during the initial cycle at 60 °C. This result agrees with our lithium ion conductivity measurement that APCE has a higher ionic conductivity than the corresponding SPE at all temperatures tested. In addition to the reduced overpotentials, the cycle stability has also been improved in APCE when compared to SPE. Because of the poor mechanical properties of PEO, especially at increased temperature (Figure S7a,d), the Li/SPE/Li cell was shorted

after merely eight cycles. For comparison, the Li/APCE/Li cell was cycled for more than 80 cycles without shorting. Note that SPE used here has same thickness of ∼60 μm as APCE (Figures S6b and S8). The difference in cycle life suggests that the rigid AAO template served as a strong backbone for APCE and helps prevent lithium dendrites from penetrating the composite electrolyte. Archer and his colleagues also demonstrated the excellent ability of AAO to stabilize lithium electrodeposition in liquid electrolytes.[65−68] The rigid AAO template also enabled the adoption of PEO with smaller molecular weight. For the cell based on APCE-1.5K-AF, the overpotential was as low as ∼40 mV at a much higher current density (0.75 mA/cm^2) and a reduced testing temperature (RT) due to its outstanding ionic conductivity. For comparison, SPE based on 1.5k PEO is mechanically soft and cannot be used.

Additionally, APCE exhibits better thermal stability than SPE. APCE did not show any changes in terms of its macroscopic morphology and mechanical hardness after baking at 80 °C for 1 h, while the sample of SPE became sticky and shrank in size (Figure S7). Combustion tests showed that SPE caught fire immediately when the touched with the flame of a lighter and only a bit of ashes were left after burning (Figure S9a,c). On the contrary, the combustion of APCE was much less violent than SPE, and the ceramic framework of APCE maintained its spatial structure after combustion although the polymer phase was burned off (Figure S9d,i). This indicates that APCE can physically block the cathode and anode from contact and prevent resultant disasters, especially under extreme conditions of burning.

Furthermore, the long-term stability of APCE was demonstrated by the fact that the ionic conductivity of APCE remained unchanged after the samples were stored for over one month (Figure 5c,d). This stability is indiscriminately shown by all ACPE based on polymers with different molecular weights and AAO with or without surface modification. This can be attributed to the fact that the structure-stable ceramic phase in APCE does not move or aggregate like randomly dispersed ceramic fillers in conventional CSPE. In other words, the fast Li$^+$ transport paths along the vertically aligned and continuous nanoscale ceramic−polymer interfaces are preserved, and thus the samples of APCE maintain their original ionic conductivity over a long time.

Composite electrolytes based on LiClO$_4$ were also prepared and investigated. They showed a similar ionic conductivity enhancing behavior to composite electrolyte based on LiTFSI (Note S7). On the one hand, the absolute ionic conductivity of APCE based on LiClO$_4$ was not as high as that of APCE based on LiTFSI because TFSI- may plasticize the polymer matrix and keep it in an amorphous state. On the other hand, due to the same reason, the ionic conductivity enhancing effects coming from the vertically aligned and continuous nanoscale interface in LiClO$_4$-based APCE is much more pronounced than that in LiTFSI based system. The above results indicated that the ionic conductivity enhancing effect coming from vertically aligned and continuous ceramic−polymer interfaces is universal, and it is not limited by the choice of materials. In future work, APCE ionic conductivity can be further improved by optimization of the choice of polymer−lithium salt−ceramic combination.

Conclusions. In summary, we developed an AAO-polymer composite electrolyte (APCE) exhibiting excellent ionic conductivity and stability, based on the idea of building densely
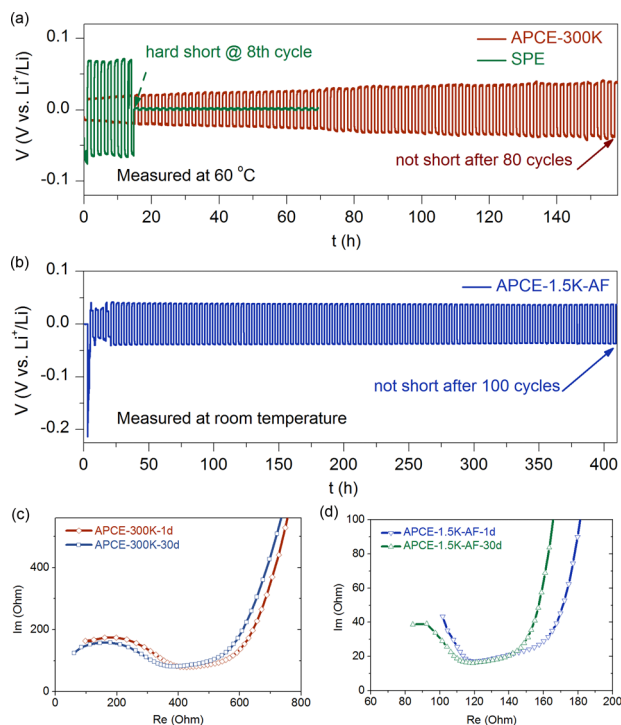
Figure 5. Galvanostatic cycling and long-term stability of APCE. (a) Voltage profiles during lithium plating/striping cycling in Li—Li symmetrical cells based on bulk SPE (green), APCE-300 K (red) measured at 60 °C with a current density of 0.25 mA/cm^2; (b) APCE-1.5K-AF measured at RT with a current density of 0.75 mA/cm^2; (c,d) electrochemical impedance spectra of APCE measured at RT after storing for 1 day and 30 days.

packed, vertically aligned, and continuous nanoscale ceramic—polymer interfaces in composite solid electrolytes. As a proof of concept, APCE achieved ionic conductivity as high as 5.82 × 10^{-4} S/cm at RT, which is, to the best of our knowledge, the highest value reported for a composite solid polymer electrolyte. We also demonstrated that APCE's superior ionic conductivity enhancement over conventional ceramic—polymer composite electrolytes originates from (i) continuous fast paths for Li$^+$ transport formed along vertically aligned interfaces, which were deduced to possess an ionic conductivity higher than 10^{-3} S/cm even at 0 °C, and (ii) the well-aligned and continuous nanoscale interfaces which diminished the reorganization of polymer segments in a more effective manner. Moreover, the ionic conductivity of APCE could be effactually tuned by modifying surface chemistry of the ceramic phase, changing the composition of the polymer phase, or varying the specific interfacial area. Thus, it is very promising to push its ionic conductivity higher than 10^{-3} S/cm to be comparable to commercial liquid electrolyte and acceptable for industrial applications, by optimization of the geometrical structure of the ceramic phase and the materials choice in the polymer—lithium salt—ceramic combination. Furthermore, as the first demonstration of composite solid electrolyte with vertically aligned and continuous nanoscale ceramic—polymer interfaces, APCE showed outstanding feasibility in Li—Li symmetrical configuration with much reduced overpotential and greatly improved cycling stability. The knowledge gained in this work paves an encouraging avenue for further developing advanced composite solid polymer electrolytes in favor of next-generation

rechargeable batteries with high levels of energy density and safety.

Materials and Methods. *Materials.* Poly(ethylene oxide) (PEO) (average M_w: 300 000), poly(ethylene glycol) (PEG) (average M_w: 1500), bis(trifluoromethane)sulfonimide lithium (LiTFSI, 99.95%), lithium perchlorate (LiClO$_4$, 99.9%), Al$_2$O$_3$ nanoparticles (<50 nm by TEM), Al$_2$O$_3$ nanowires (diameter, 2−6 nm; L, 200−400 nm), and acetonitrile (anhydrous, 99.8%) were purchased from Sigma-Aldrich. Anodized aluminum oxide discs (AAO discs, diameter = 13 mm) were purchased from Whatman plc (pore size ∼200 nm) and Shenzhen Top-membranes Technology Co., Ltd. (pore size ∼90 nm and 40 nm). PEO, PEG, LiTFSI, and LiClO$_4$ were dried at 60 °C under vacuum for 24 h and subsequently stored in an argon filled glovebox overnight prior to use. AAO discs were cleaned by oxygen plasma to remove possible surface contaminations before use.

Preparation of Solid Polymer Electrolyte (SPE) Membranes. LiTFSI and PEO ([EO]/[Li] = 16:1) were successively added into acetonitrile with a concentration of ∼18 wt %. The mixture was mechanically stirred at RT for 16 h and then cast onto PTFE substrate using a doctor blade with a gap of 50 mils. After drying at 40 °C in ambient environment for 2 h, a freestanding membrane with a thickness of ∼60 μm was peeled off from the PTFE substrate. The obtained SPE membrane was placed in a vacuum oven at 60 °C for 24 h and then baked in an argon filled glovebox (content of H$_2$O, O$_2$ < 1 ppm) at 80 °C for 48 h to remove the solvent and trace amount of water. The SPE membranes based on PEO and LiClO$_4$ ([EO]/[Li] = 12:1) were also prepared using this procedure.

Preparation of Composite Solid Polymer Electrolyte (CSPE) Membranes. The procedure for preparing PEO-LiTFSI-Al$_2$O$_3$ CSPE membranes is similar to SPE membrane. Nanoparticles (NPs) or nanowires (NWs) of Al$_2$O$_3$ were introduced into the SPE by adding NPs or NWs into the acetonitrile solution of LiTFSI and PEO.

Surface Modification of AAO Discs by Atomic Layer Deposition (ALD). ALD deposition of AlF$_3$ films on AAO substrates was done using a Savannah S100 ALD system (Ultratech/Cambridge Nanotech). Typical AlF$_3$ ALD coating consists of alternating introduction of TiF$_4$ and AlCl$_3$ precursors as F and Al sources. The deposition was performed using an exposure mode to ensure high uniformity on high surface area AAO substrates. A total of 100 ALD cycles were applied for all AAO samples. All depositions were performed at 250 °C. Both TiF$_4$ and AlCl$_3$ precursors were heated to 115 °C. High purity argon was used as carrier and purging gas.

Preparation of AAO—Polymer Composite Electrolyte (APCE). AAO—polymer composite electrolyte was prepared by melt infiltration of polymer electrolyte into vertically aligned through channels of AAO disc. For the preparation of APCE based on PEO (M_w: 300 000), the as-prepared PEO-LiTFSI SPE membrane was thermally laminated onto the top of AAO discs at 80 °C. The double layered precursor was then transferred into a tube furnace. The precursor was heated up under active vacuum with a detailed temperature ramping program: RT to 150 °C, 20 min; 150 to 165 °C, 10 min; keep at 165 °C for 2 h; 165 to 205 °C, 20 min; 205 to 215 °C, 10 min; keep at 215 °C for 12 h; quench to RT. The water absorbed during precursor preparation was removed at 165 °C. At 205 °C, the SPE membrane was melted and infiltrated into the porous channels of AAO discs. After cooling down, the bulk polymer left on the top of AAO disc was removed using a razor

blade and the surface of the AAO disc was cleaned by swab. The APCE sample was placed in a vacuum oven at 60 °C for 24 h and then baked in an argon filled glovebox (content of H_2O, $O_2 < 1$ ppm) at 80 °C for 48 h to remove solvent and trace amount of water. For the preparation of APCE based on PEG (M_w. 1500), LiTFSI and PEG ([EO]/[Li] = 16:1) were successively added into acetonitrile with a concentration of ~18 wt %. The mixture was mechanically stirred at RT for 16 h and then poured into a glass Petri dish. After drying at 85 °C for 2 h, most of the solvent was evaporated and the resultant viscous paste in the Petri dish was further dried under vacuum overnight. AAO disc was then placed into the Petri dish containing the homogeneous mixture of PEG and LiTFSI. The Petri dish was kept in vacuum at 60 °C for 24 h and at RT for another 24 h. AAO disc was carefully removed from the Petri dish. The bulk polymer remaining on the surface of AAO disc was removed using a razor blade and the surface of the AAO disc was wiped by swab. The APCE sample was baked in an argon-filled glovebox (content of H_2O, $O_2 < 1$ ppm) at 35 °C for 1 week to remove the solvent and the trace amount of water. The APCE samples based on surface-modified AAO discs or using $LiClO_4$ as the lithium salt ([EO]/[Li] = 12:1) were also prepared by this procedure. The melt infiltration temperature for the PEO−$LiClO_4$ SPE membrane is 215 °C. A proper lithium salt concentration was selected based on our experiments (see Note S8). In addition, previous result has also shown when a high lithium salt concentration would also lead to low lithium ion conductivity.[69]

Characterizations. SEM images and EDX data were taken using a FEI Nova NanoSEM 450 equipped with an EDX detector. The FTIR spectra were measured with a Nicolet iS5 FT-IR Spectrometer in a glovebox (content of H_2O, $O_2 < 1$ ppm). Differential scanning calorimetry measurements were conducted using TA Instrument Q2000. Samples (~10 mg) placed in aluminum pans with lids and an empty reference pan were heated from RT to 110 °C at the rate of 30 K/min and then cooled down from 110 °C to 0 °C or −40 °C at the rate of 5 K/min, all while under flowing N_2 gas (50 mL/min). The DSC traces were recorded during cool down.

Electrochemical Measurements. Ionic conductivity was measured by sandwiching solid electrolyte into two stainless steel (SS) blocking electrodes using electrochemical impedance spectroscopy. The frequency range was set from 100 mHz to 1 MHz. To lower the contact resistance, a gold electrode with diameter of 4.5 mm and thickness of 100 nm, was sputtered onto the surfaces of APCE. SS/electrolyte/SS symmetrical cells were kept at each temperature for 1 h to achieve thermal equilibrium prior to the EIS measurement. The bulk alumina walls of AAO are inert for Li^+ conduction. The active surface area (the area of gold electrode times the porosities of AAO discs) was used to calculate the ionic conductivity of APCE. Ionic transport number was estimated in SS/electrolyte/SS cells by means of direct current polarization with a fixed bias of 80 mV across the symmetrical cell. The inhibition of lithium dendrite penetration was studied in Li/APCE/Li and Li/SPE/Li cells by means of galvanostatic cycling. Electrochemical measurements were conducted using a biologic VMP3 system and an 8-channel Land battery test system. The temperature of the cells was controlled by an environmental chamber (BTU-133, ESPEC North American, Inc.).

■ ASSOCIATED CONTENT

Ⓢ Supporting Information

The Supporting Information is available free of charge on the ACS Publications website at DOI: 10.1021/acs.nanolett.8b01111.

> Calculations of specific surface area, crystallinity, and ionic transport number of composite solid polymer electrolytes involved in this study, photographs of heating and combustion tests of SPE and APCE, details of the analysis of the interfacial ionic conduction of APCE, and supplementary data of electrochemical, structural, and thermal analyses of the presented samples (PDF)

■ AUTHOR INFORMATION

Corresponding Authors
*E-mail: xyg@uestc.edu.cn.
*E-mail: yicui@stanford.edu.

ORCID ◉
Xiaokun Zhang: 0000-0002-9399-8847
Jin Xie: 0000-0002-6270-1465
Dingchang Lin: 0000-0002-9354-5952
Wei Liu: 0000-0002-6206-8321
Allen Pei: 0000-0001-8930-2125
Hongxia Wang: 0000-0003-0720-3305
Kai Liu: 0000-0003-3362-180X
Yong Xiang: 0000-0002-6667-3473
Yi Cui: 0000-0002-6103-6352

Author Contributions
[⊥]Xiaokun Zhang and Jin Xie contributed equally to this study. X.Z., J.X., Y.X., and Y.C. conceived the concept and designed the experiments. X.Z. and J.X. carried out the materials fabrication and electrochemical measurements with the assistance from Y.L., W.L., and H.W. F.S. and A.P. performed the FTIR measurements. D.L. and Y.L. performed DSC measurements. Y.G. conducted the EDS characterization. K.L. helped with the SEM characterizations. X.Z., J.X., Y.X., and Y.C. wrote the paper. All the authors discussed the results and commented on the manuscript.

Notes
The authors declare no competing financial interest.

■ REFERENCES

(1) Armand, M.; Tarascon, J. M. *Nature* **2008**, *451*, 652−657.
(2) Tarascon, J. M.; Armand, M. *Nature* **2001**, *414*, 359−367.
(3) Manthiram, A. *J. Phys. Chem. Lett.* **2011**, *2*, 176−184.
(4) Jeong, G.; Kim, Y.-U.; Kim, H.; Kim, Y.-J.; Sohn, H.-J. *Energy Environ. Sci.* **2011**, *4*, 1986−2002.
(5) Xu, K. *Chem. Rev.* **2004**, *104*, 4303−4418.
(6) Xu, K. *Chem. Rev.* **2014**, *114*, 11503−11618.
(7) Hallinan, D. T.; Balsara, N. P. *Annu. Rev. Mater. Res.* **2013**, *43*, 503−525.

(8) Meyer, W. H. *Adv. Mater.* **1998**, *10*, 439−448.

(9) Liu, Y.; Lin, D.; Yuen, P. Y.; Liu, K.; Xie, J.; Dauskardt, R. H.; Cui, Y. *Adv. Mater.* **2017**, *29*, 1605531.

(10) Lin, D.; Liu, Y.; Cui, Y. *Nat. Nanotechnol.* **2017**, *12*, 194−206.

(11) Quartarone, E.; Mustarelli, P. *Chem. Soc. Rev.* **2011**, *40*, 2525−2540.

(12) Kato, Y.; Hori, S.; Saito, T.; Suzuki, K.; Hirayama, M.; Mitsui, A.; Yonemura, M.; Iba, H.; Kanno, R. *Nat. Energy* **2016**, *1*, 16030.

(13) Wang, Y.; Richards, W. D.; Ong, S. P.; Miara, L. J.; Kim, J. C.; Mo, Y.; Ceder, G. *Nat. Mater.* **2015**, *14*, 1026−31.

(14) Zhao, C.-Z.; Zhang, X.-Q.; Cheng, X.-B.; Zhang, R.; Xu, R.; Chen, P.-Y.; Peng, H.-J.; Huang, J.-Q.; Zhang, Q. *Proc. Natl. Acad. Sci. U. S. A.* **2017**, *114*, 11069−11074.

(15) Yang, C.; Liu, B.; Jiang, F.; Zhang, Y.; Xie, H.; Hitz, E.; Hu, L. *Nano Res.* **2017**, *10*, 4256−4265.

(16) Ma, C.; Cheng, Y. Q.; Chen, K.; Li, J. C.; Sumpter, B. G.; Nan, C. W.; More, K. L.; Dudney, N. J.; Chi, M. F. *Adv. Energy Mater.* **2016**, *6*, 1600053.

(17) Tong, X.; Thangadurai, V.; Wachsman, E. D. *Inorg. Chem.* **2015**, *54*, 3600−3607.

(18) Kamaya, N.; Homma, K.; Yamakawa, Y.; Hirayama, M.; Kanno, R.; Yonemura, M.; Kamiyama, T.; Kato, Y.; Hama, S.; Kawamoto, K.; Mitsui, A. *Nat. Mater.* **2011**, *10*, 682−686.

(19) Yu, Z.; Shang, S.-L.; Seo, J.-H.; Wang, D.; Luo, X.; Huang, Q.; Chen, S.; Lu, J.; Li, X.; Liu, Z.-K.; Wang, D. *Adv. Mater.* **2017**, *29*, 1605561.

(20) Marcinek, M.; Zalewska, A.; Żukowska, G.; Wieczorek, W. *Solid State Ionics* **2000**, *136−137*, 1175−1179.

(21) Li, Q.; Jiao, S.; Luo, L.; Ding, M. S.; Zheng, J.; Cartmell, S. S.; Wang, C.-M.; Xu, K.; Zhang, J.-G.; Xu, W. *ACS Appl. Mater. Interfaces* **2017**, *9*, 18826−18835.

(22) Lin, Y.; Wang, X.; Liu, J.; Miller, J. D. *Nano Energy* **2017**, *31*, 478−485.

(23) Srivastava, S.; Schaefer, J. L.; Yang, Z.; Tu, Z.; Archer, L. A. *Adv. Mater.* **2014**, *26*, 201−234.

(24) Manuel Stephan, A.; Nahm, K. S. *Polymer* **2006**, *47*, 5952−5964.

(25) Liu, W.; Liu, N.; Sun, J.; Hsu, P.-C.; Li, Y.; Lee, H.-W.; Cui, Y. *Nano Lett.* **2015**, *15*, 2740−2745.

(26) Zhai, H.; Xu, P.; Ning, M.; Cheng, Q.; Mandal, J.; Yang, Y. *Nano Lett.* **2017**, *17*, 3182−3187.

(27) Croce, F.; Appetecchi, G. B.; Persi, L.; Scrosati, B. *Nature* **1998**, *394*, 456−458.

(28) Vaia, R. A.; Vasudevan, S.; Krawiec, W.; Scanlon, L. G.; Giannelis, E. P. *Adv. Mater.* **1995**, *7*, 154−156.

(29) Kumar, B.; Scanlon, L. G.; Spry, R. J. *J. Power Sources* **2001**, *96*, 337−342.

(30) Lin, D.; Liu, W.; Liu, Y.; Lee, H. R.; Hsu, P. C.; Liu, K.; Cui, Y. *Nano Lett.* **2016**, *16*, 459−65.

(31) Wieczorek, W.; Florjanczyk, Z.; Stevens, J. R. *Electrochim. Acta* **1995**, *40*, 2251−2258.

(32) Borkowska, R.; Reda, A.; Zalewska, A.; Wieczorek, W. *Electrochim. Acta* **2001**, *46*, 1737−1746.

(33) Wang, Z.; Huang, X.; Chen, L. *Electrochem. Solid-State Lett.* **2003**, *6*, E40−E44.

(34) Croce, F.; Persi, L.; Scrosati, B.; Serraino-Fiory, F.; Plichta, E.; Hendrickson, M. A. *Electrochim. Acta* **2001**, *46*, 2457−2461.

(35) Kasemagi, H.; Klintenberg, M.; Aabloo, A.; Thomas, J. O. *J. Mater. Chem.* **2001**, *11*, 3191−3196.

(36) Johansson, P.; Jacobsson, P. *Solid State Ionics* **2004**, *170*, 73−78.

(37) Krutyeva, M.; Wischnewski, A.; Monkenbusch, M.; Willner, L.; Maiz, J.; Mijangos, C.; Arbe, A.; Colmenero, J.; Radulescu, A.; Holderer, O.; Ohl, M.; Richter, D. *Phys. Rev. Lett.* **2013**, *110*, 108303.

(38) Fu, K.; Gong, Y.; Dai, J.; Gong, A.; Han, X.; Yao, Y.; Wang, C.; Wang, Y.; Chen, Y.; Yan, C.; Li, Y.; Wachsman, E. D.; Hu, L. *Proc. Natl. Acad. Sci. U. S. A.* **2016**, *113*, 7094−7099.

(39) Liu, W.; Lee, S. W.; Lin, D.; Shi, F.; Wang, S.; Sendek, A. D.; Cui, Y. *Nat. Energy* **2017**, *2*, 17035.

(40) Martín, J.; Mijangos, C. *Langmuir* **2009**, *25*, 1181−1187.

(41) Martin, J.; Vazquez, M.; Hernandez-Velez, M.; Mijangos, C. *Nanotechnology* **2008**, *19*, 175304.

(42) Xie, J.; Sendek, A. D.; Cubuk, E. D.; Zhang, X.; Lu, Z.; Gong, Y.; Wu, T.; Shi, F.; Liu, W.; Reed, E. J.; Cui, Y. *ACS Nano* **2017**, *11*, 7019−7027.

(43) Bakker, A.; Gejji, S.; Lindgren, J.; Hermansson, K.; Probst, M. M. *Polymer* **1995**, *36*, 4371−4378.

(44) Porcarelli, L.; Gerbaldi, C.; Bella, F.; Nair, J. R. *Sci. Rep.* **2016**, *6*, 19892.

(45) Cantwell, P. R.; Tang, M.; Dillon, S. J.; Luo, J.; Rohrer, G. S.; Harmer, M. P. *Acta Mater.* **2014**, *62*, 1−48.

(46) Weston, J. E.; Steele, B. C. H. *Solid State Ionics* **1982**, *7*, 75−79.

(47) Kim, J.-W.; Ji, K.-S.; Lee, J.-P.; Park, J.-W. *J. Power Sources* **2003**, *119-121*, 415−421.

(48) Dygas, J. R.; Misztal-Faraj, B.; Florjańczyk, Z.; Krok, F.; Marzantowicz, M.; Zygadło-Monikowska, E. *Solid State Ionics* **2003**, *157*, 249−256.

(49) Ramesh, S.; Yuen, T. F.; Shen, C. J. *Spectrochim. Acta, Part A* **2008**, *69*, 670−5.

(50) Marcinek, M.; Ciosek, M.; Zukowska, G.; Wieczorek, W.; Jeffrey, K. R.; Stevens, J. R. *Solid State Ionics* **2004**, *171*, 69−80.

(51) Stygar, J.; Żukowska, G.; Wieczorek, W. *Solid State Ionics* **2005**, *176*, 2645−2652.

(52) Sim, L. H.; Gan, S. N.; Chan, C. H.; Yahya, R. *Spectrochim. Acta, Part A* **2010**, *76*, 287−292.

(53) Rey, I.; Lassègues, J. C.; Grondin, J.; Servant, L. *Electrochim. Acta* **1998**, *43*, 1505−1510.

(54) Wen, S. J.; Richardson, T. J.; Ghantous, D. I.; Striebel, K. A.; Ross, P. N.; Cairns, E. J. *J. Electroanal. Chem.* **1996**, *408*, 113−118.

(55) Suzuki, Y.; Duran, H.; Steinhart, M.; Butt, H.-J.; Floudas, G. *Soft Matter* **2013**, *9*, 2621−2628.

(56) Eltanany, G.; Rudiger, S.; Kemnitz, E. *J. Mater. Chem.* **2008**, *18*, 2268−2275.

(57) Krahl, T.; Kemnitz, E. *Catal. Sci. Technol.* **2017**, *7*, 773−796.

(58) Zheng, J.; Gu, M.; Xiao, J.; Polzin, B. J.; Yan, P.; Chen, X.; Wang, C.; Zhang, J.-G. *Chem. Mater.* **2014**, *26*, 6320−6327.

(59) Guan, Y.; Liu, G.; Gao, P.; Li, L.; Ding, G.; Wang, D. *ACS Macro Lett.* **2013**, *2*, 181−184.

(60) Mi, C.; Zhou, J.; Ren, Z.; Li, H.; Sun, X.; Yan, S. *Polym. Chem.* **2016**, *7*, 410−417.

(61) Linegar, K. L.; Adeniran, A. E.; Kostko, A. F.; Anisimov, M. A. *Colloid J.* **2010**, *72*, 279−281.

(62) Gurnev, P. A.; Stanley, C. B.; Aksoyoglu, M. A.; Hong, K.; Parsegian, V. A.; Bezrukov, S. M. *Macromolecules* **2017**, *50*, 2477−2483.

(63) Sung, J. H.; Lee, D. C.; Park, H. J. *Polymer* **2007**, *48*, 4205−4212.

(64) Devanand, K.; Selser, J. C. *Macromolecules* **1991**, *24*, 5943−5947.

(65) Tu, Z.; Zachman, M. J.; Choudhury, S.; Wei, S.; Ma, L.; Yang, Y.; Kourkoutis, L. F.; Archer, L. A. *Adv. Energy Mater.* **2017**, *7*, 1602367.

(66) Tu, Z.; Lu, Y.; Archer, L. *Small* **2015**, *11*, 2631−2635.

(67) Lu, Y.; Tu, Z.; Archer, L. A. *Nat. Mater.* **2014**, *13*, 961−969.

(68) Tu, Z.; Kambe, Y.; Lu, Y.; Archer, L. A. *Adv. Energy Mater.* **2014**, *4*, 1300654.

(69) Hsu, W.-L.; Harvie, D. J. E.; Davidson, M. R.; Dunstan, D. E.; Hwang, J.; Daiguji, H. *J. Phys. Chem. C* **2017**, *121*, 20517−20523.